Available online at www.sciencedirect.com
ScienceDirect
International Journal of Thermal Sciences 47 (2008) 709–722
International Journal of Thermal Sciences
www.elsevier.com/locate/ijts

Weakly nonlinear interaction of mixed convection patterns in porous media heated from below

A. Delache, M.N. Ouarzazi *

Laboratoire de Mécanique de Lille, UMR CNRS 8107, USTL, bd. Paul Langevin, 59655 Villeneuve d'Ascq cedex, France

Received 26 December 2006; received in revised form 22 May 2007; accepted 10 June 2007

Available online 26 July 2007

Abstract

Available experimental data and linear stability analysis indicate that the secondary flow configurations of convection in a rectangular duct with a saturated porous medium heated from below and through which an axial flow is maintained are down-stream moving three-dimensional rolls (T modes) for low Péclet number or stationary longitudinal rolls (L rolls) otherwise. In this paper, a weakly nonlinear analysis is used and coupled envelope equations are derived to study the competition between T modes and L rolls in the neighborhood of a double bifurcation point where these two convective configurations become simultaneously unstable. An entire stability diagram of homogeneous nonlinear states is obtained and the evaluated mean heat transfer is found to compare well with experimental data. Moreover parameter boundaries for absolute and convective instability of the basic state with respect to T modes and L rolls are determined. In the case of convective instability, we obtain an analytical criterion which specifies conditions about the observability of either T modes or L rolls at the onset of convection. This criterion implies an explicit relation between the spatial growth of the two patterns and the magnitude of their inlet forcing. Suitable numerical simulations of the envelope equations perfectly validate the derived analytical criterion. On the other hand, in the region of absolute instability, it is found that the L roll/T mode transition observed in early experiments, is ascribed to the transition to absolute instability of the basic state with respect to L rolls. Additionally, numerical solutions as well as both temporal and spatial nonlinear stability theory demonstrate that the mixed mode is an unstable state in agreement with experimental results. Throughout this paper, major similarities as well as differences with the corresponding problem in pure fluids are particularly highlighted.

Keywords: Mixed convection; Porous media; Nonlinear pattern selection; Inlet forcing

1. Introduction

While the problem of free-convective flows in porous media has been extensively investigated [1], little attention has been devoted to the mixed convection in a differentially heated porous layer with a superimposed through-flow. As far as the authors are aware, the numerical investigation of mixed convection flows in porous media conducted by Dufour and Néel [2] is the only published paper focusing on the nonlinear properties of two-dimensional patterns. Within the framework of Darcy's law, these authors demonstrated that the nonlinear two-dimensional solutions are saturated travelling rolls in the bulk region with envelopes in the form of fronts near the entrance zone. The global frequency, the wavelength and the phase velocity of the travelling rolls were also computed in [2]. From the linear point of view, temporal stability analysis of the problem of mixed convection in porous media of the kind performed by some investigators (Prats [3], Rees [4], Delache et al. [5]) consider perturbations which amplify in time, starting from an initial spatially periodic perturbation, i.e. they assume that the perturbation wave number k is real while its frequency ω is complex. Such analysis allow us to distinguish between stable and unstable configurations without taking into account an important feature inherent to open flow systems, namely the spatial propagation of the unstable flow structures. In fact, it is well known that instability is described as convective provided an initial small perturbation localized in space is convected downstream leaving the flow domain unperturbed, as time tends to infinity. On the contrary, instability is described

* Corresponding author. Tel.: +33320434261; fax: +33320337088.
E-mail address: najib.ouarzazi@univ-lille1.fr (M.N. Ouarzazi).

1290-0729/$ – see front matter
doi:10.1016/j.ijthermalsci.2007.06.015

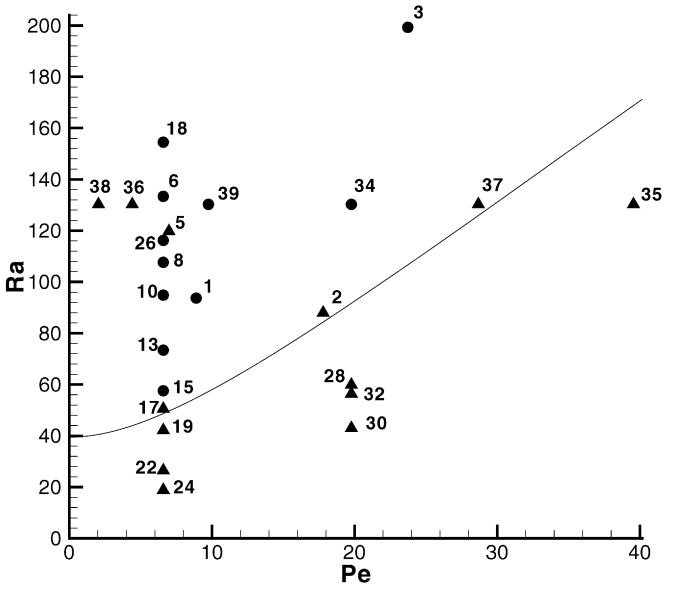

Fig. 1. Flow regime map in the (*Pe*, *Ra*) plane for pattern observed in [10–12] with glass beads of diameter 4 mm and water: T modes (•) and L rolls (▲). Experimental runs are indicated by the numbers. The missed numbers are in a fluctuating region. The curve represents the border between convective and absolute instability predicted theoretically in [9].

as absolute whenever the initial small localized perturbation expands both in the upstream and downstream directions as time grows, affecting eventually the whole flow domain. Such a fundamental distinction was originally proposed in the field of plasma physics by Briggs [6] and Bers [7] and has since been developed in hydrodynamic stability by several authors (see Huerre and Monkewitz [8]). The analysis presented by Delache et al. [9] dealt with a linear spatio-temporal stability analysis to discriminate between convective and absolute nature of the instability of the basic flow with respect to moving three-dimensional modes (T modes) as well as to stationary longitudinal rolls (L rolls) with their rotation axes parallel to the through-flow direction. In relation to experiments, the most interesting result stemming from this analysis is that the border between the convective and the absolute instability of moving T modes corresponds perfectly to the experimentally observed transition from T modes to L rolls and vice versa. This feature is illustrated in Fig. 1 where we reproduce the flow regime map in the filtration Rayleigh–Péclet number plane (*Pe*, *Ra*) of different patterns observed in laminar mixed convection regime i.e. $Ra < 260$ (Combarnous [10], Combarnous and Bia [11], Combarnous and Bories [12]) as well as the convective/absolute instability boundaries of T modes as they have been determined in [9]. Having ascertained that the experimentally observed transition between L rolls and T modes is ascribed to the transition to absolute instability, experimental results raise further questions:

(i) by which physical mechanisms the system preferentially selects L rolls rather than T modes in the convectively unstable region (i.e. region below the curve of Fig. 1)?

(ii) why experiments [10–12]) revealed the existence of a region associated with either L rolls (points 5, 36, 38 of Fig. 1) or T modes in the absolutely unstable domain (i.e. region above the curve of Fig. 1)?

(iii) why some temperature recordings [10–12] have shown the coexistence of L rolls and T modes, albeit in different parts of the medium?

(iv) can theory predict the experimental results which revealed that the existence of a horizontal through-flow does not modify the vertical mean heat transfer compared with natural convection?

The main purpose of this paper is to provide some answers to these questions. This task will be accomplished by taking into account two major ingredients, namely the nonlinearities of the problem and the presence of a persistent forcing of an initial perturbation. Therefore this work is a natural extension to [9].

The temporal linear stability analysis performed in [5,9] concluded that there exists a critical Reynolds number Re_K^* based on the permeability of the medium in such a way that for $Re_K < Re_K^*$ the T modes propagating with phase velocity equal to *Pe* become unstable first at Ra_c^{3D}. While for $Re_K > Re_K^*$ the most unstable disturbances are L rolls ($Ra_c^{\parallel} < Ra_c^{3D}$). For $Re_K = Re_K^*$ and $Ra_c^{3D} = Ra_c^{\parallel} = Ra^*$ both the T modes and the L rolls become simultaneously unstable and the linear theory fails to predict the bifurcation processes and to elucidate the dominant convection patterns. Therefore nonlinear stability analysis is needed to study the competition between T modes and L rolls in the neighborhood of the double bifurcation point (Re_K^*, Ra^*). It should be emphasized that there is a close analogy between the present porous medium and the pure-fluid case which is generally known as the Poiseuille–Rayleigh–Bénard ($P.R.B.$) problem (see a recent bibliographical review on the $P.R.B.$ flows by Nicolas [13]). We believe that any insight gained into the qualitative features of $P.R.B.$ problem is a valuable aid to our understanding of the mixed convection in porous media and conversely. In $P.R.B.$ problem the nonlinear interaction between T modes and the L rolls was investigated notably by Brand et al. [14] and Müller et al. [15]. They applied a weakly nonlinear theory for perturbations which modulated both on time and space and obtained a coupled envelope equations. As pointed out by Kato and Fujimura [16], the disagreement between the predictions of [14] and [15] concerning the stability of a mixed mode comes from the difference of the coefficients of nonlinear interaction terms in their respective model. Therefore Kato and Fujimura [16] used the two time-scale analysis and derived rigorously a set of two coupled Landau equations, each of them describing the time evolution of L rolls and T modes respectively. Their reduced model is adequate to predict stable patterns for given sets of parameters but it does not take into account the modulation of the convective patterns which occur on a spatial scale. On the other hand, in a recent paper dealing with $P.R.B.$ problem in the case of infinite lateral extent of the fluid medium, Carrière et al. [17] derived in a consistent manner envelope equations describing separately L rolls for O(1) Reynolds numbers and T modes in

the limit of small Reynolds numbers and examined their stability properties. In this paper a systematic derivation of coupled Ginzburg–Landau equations valid in the neighborhood of the double bifurcation point (Re_K^*, Ra^*) will be presented and the stability of its homogeneous solutions will be studied. In the framework of the derived reduced model, the mean heat transfer is evaluated and compared to experimental data. Moreover an analytical analysis and a series of suitable numerical simulations of the coupled Ginzburg–Landau equations are performed to elucidate, in relation to experiments, the role of inlet perturbations upon the selection of patterns in the unstable regions.

2. Mathematical formulation

All results are obtained for an isotropic and homogeneous porous layer of infinite horizontal extent of rectangular cross section with thickness H and width aH saturated by a fluid. The medium is heated from below and cooled from the top with impermeable and insulated lateral sides. The bottom wall is at a uniform temperature T_0, while the top wall is at a uniform, but lower, temperature T_1. The solid matrix is supposed to be in thermal equilibrium with the fluid. Furthermore, we consider that a through-flow is driven by a pressure gradient in the x-direction. The Forchheimer correction to Darcy's law is used and the Boussinesq approximation is employed. We choose H, $H^2(\rho c)/k_{\mathrm{stg}}$, $T_0 - T_1$, $k_{\mathrm{stg}}/(H(\rho c)_f)$ and $k_{\mathrm{stg}}\mu/(K(\rho c)_f)$ as references for length, time, temperature, filtration velocity and pressure. Here, k_{stg}, (ρc), $(\rho c)_f$, K and μ are, respectively, the effective stagnant thermal conductivity, the overall heat capacity of the porous medium per unit volume, the heat capacity per unit volume of the fluid alone, the permeability of the medium and the viscosity of the fluid. Under these conditions the dimensionless equations governing the flow are

$$\begin{aligned}
&\vec{\nabla}\cdot\vec{V} = 0\\
&\vec{V} + F\|\vec{V}\|\vec{V} = -\vec{\nabla}P + Ra\,T\vec{e}_z\\
&\frac{\partial T}{\partial t} = -\vec{V}\cdot\vec{\nabla}T + \vec{\nabla}^2 T
\end{aligned} \tag{1}$$

with boundary conditions:

$$\vec{V}\cdot\vec{e}_z = 0 \quad \text{at } z = 0, 1$$

$$\vec{V}\cdot\vec{e}_y = 0 \quad \text{at } y = 0, a \tag{2}$$

$$T = 1 \quad \text{at } z = 0; \qquad T = 0 \quad \text{at } z = 1$$

$$\frac{\partial T}{\partial y} = 0 \quad \text{at } y = 0, a \tag{3}$$

with an imposed through-flow:

$$\int_0^a \int_0^1 \vec{V}\cdot\vec{e}_x \,\mathrm{d}y\,\mathrm{d}z = a\,Pe \tag{4}$$

where $P, \vec{V}, T, \vec{e}_z$ are the pressure, the filtration velocity, the temperature and the vertical upwards unit vector respectively.

The non-dimensional parameters are: the filtration Rayleigh number $Ra = Kg\alpha H(T_0 - T_1)(\rho c)_f/k_{\mathrm{stg}}\nu$, the Péclet number $Pe = UH(\rho c)_f/k_{\mathrm{stg}}$, the lateral aspect ratio a and the Forchheimer number $F = C[K^{1/2}k_{\mathrm{stg}}/H\nu(\rho c)_f]$ which represents the nonlinear drag effect due to the solid matrix.

U, g, ν, α and C are respectively, the average filtration velocity imposed at the entrance of the channel, the gravitational acceleration, the kinematic viscosity, the volumetric coefficient of thermal expansion and a dimensionless form-drag constant.

A basic solution of the problem (1)–(4) is a combination of a vertical thermal stratification and a homogeneous flow in the $\vec{e}_x$ direction:

$$\begin{aligned}
&\vec{V}_b = Pe\cdot\vec{e}_x, \quad T_b = 1 - z \quad \text{and}\\
&P_b = Ra\big(z - z^2/2\big) - Pe\big(1 + Re_K\big)x
\end{aligned} \tag{5}$$

where $Re_K = F\,Pe = C(UK^{1/2}/\nu)$ is a Reynolds number based on the permeability of the medium. The Darcy model is recovered if $Re_K = 0$ (i.e. $F = 0$).

Now, as usual, the stability of the basic solution (5) is studied by super-imposing general perturbations onto the basic solution:

$$\begin{aligned}
(\vec{V}, T, P) = \big(&\vec{V}_b + \vec{v}(x, y, z, t), T_b + \theta(x, y, z, t),\\
&P_b + p(x, y, z, t)\big)
\end{aligned} \tag{6}$$

Substitution of (6) into (1), yields a set of flow perturbation equations which can be written in a compact form:

$$(I\,\partial/\partial t + L)\boldsymbol{\Phi} = N(\boldsymbol{\Phi}, \boldsymbol{\Phi}) \tag{7}$$

Where the vector $\boldsymbol{\Phi}$ is simply $\boldsymbol{\Phi} = [u, v, w, \theta, p]^T$. The expressions of the linear operators I and L and the nonlinear part of the dynamics N are given in Appendix A.

The system (7) must be supplemented with boundary conditions:

$$w = \theta = 0 \quad \text{at } z = 0, 1 \tag{8}$$

$$v = \partial\theta/\partial y = 0 \quad \text{at } y = 0, a \tag{9}$$

It has been demonstrated in [5,9] that for a Rayleigh number larger than a critical value Ra_c which depends on Reynolds number Re_K the basic state (5) is unstable. The linear theory shows that in this case convective configurations with exponentially growing amplitudes will develop in the form of:

(i) oscillatory three-dimensional instabilities (T modes) at $Ra = Ra_c^{3\mathrm{D}}$ for $Re_K < Re_K^*$ (see Fig. 2 for an illustration),

(ii) stationary longitudinal rolls (L rolls) with their rotation axes parallel to the through-flow direction at $Ra = Ra_c^{\|}$ for $Re_K > Re_K^*$, where,

$$Ra_c^{3\mathrm{D}} = \Big(\sqrt{1 + Re_K\,(1 - m_{3\mathrm{D}}^2/a^2)} + \sqrt{1 + 2\,Re_K}\,\Big)^2\pi^2 \tag{10}$$

and

$$Ra_c^{\|} = \pi^2(a/m_{\|} + m_{\|}/a)^2(1 + Re_K) \tag{11}$$

The two neutral curves intersect when $Ra_c^{3\mathrm{D}} = Ra_c^{\|} = Ra^*$ and $Re_K = Re_K^*$.

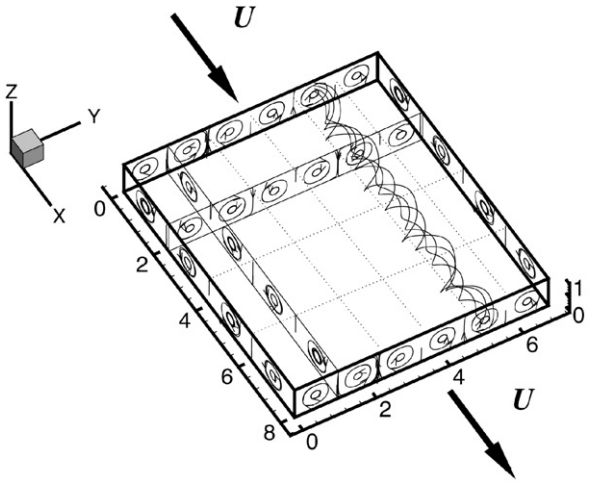

Fig. 2. Example of moving three-dimensional modes: four trajectories of fluid particles are shown as they are computed in a fixed reference frame together with streamlines in (x, z) and (y, z) planes determined in a frame moving with the main velocity U. The arrows indicate the through-flow direction.

We recall that this linear description is only valid in the initial growth stage, where the amplitudes are infinitesimally small. If we want to describe the nonlinear dynamic behavior, we must take into account the nonlinear interactions between the linearly unstable modes. A detailed analysis is possible if the Rayleigh number is only slightly larger than its critical value. This weakly nonlinear analysis has been applied to various physical systems such as Rayleigh–Bénard convection [18], Poiseuille flow [19], binary fluid convection in porous media [20], nonlinear optics [21] or more recently, Poiseuille–Rayleigh–Bénard problem [17].

The purpose of the following section is to derive two coupled envelope equations, the so called coupled Ginzburg–Landau equations, describing the interaction between (see Appendix A):

$$1)\ T \text{ modes:}\quad w = A\mathrm{e}^{\mathrm{i}(kx-\omega t)}\sin[\pi z]\cos\left[\frac{m}{a}\pi y\right] \quad \text{with } k \neq 0 \quad \text{and} \tag{12}$$

$$2)\ L \text{ rolls:}\quad w = B\sin[\pi z]\cos\left[\frac{m}{a}\pi y\right] \tag{13}$$

in the neighborhood of a double bifurcation point (Re_K^*, Ra^*) where, according to the linear theory, the two convective configurations simultaneously become unstable.

3. Weakly nonlinear analysis

3.1. Derivation of coupled envelope equations

In order to derive the coupled envelope equations we restrict ourselves to Rayleigh number Ra and Reynolds number Re_K for which holds:

$$Ra = Ra^* + \varepsilon^2 Ra_2 \quad \text{and} \quad Re_K = Re_K^* + \varepsilon^2 Re_2 \quad \text{where } \varepsilon \ll 1,\ Ra_2 = \mathrm{O}(1) \text{ and } Re_2 = \mathrm{O}(1) \tag{14}$$

From mathematical point of view parameter ε should be 'small enough' in order to be able to perform a perturbation analysis. A look at the modes which experience growth above threshold will give us the right scalings for the slow time and space variables. These scalings can be estimated by expanding the complex frequency ω obtained by a linear stability analysis in a Taylor series near (Re_K^*, Ra^*, k_c^*):

$$\omega - \omega_c^* = (\partial\omega/\partial k)_c^*(k-k_c^*) + (\partial^2\omega/\partial k^2)_c^*(k-k_c^*)^2/2 + (\partial\omega/\partial Ra)_c^*(Ra-Ra^*) + (\partial\omega/\partial Re_K)_c^*(Re_K - Re_K^*) + \cdots \tag{15}$$

where $^*_c$ means evaluation at critical conditions exactly at the double bifurcation point (Re_K^*, Ra^*). We recall that while for T modes $\omega_c^* = k_c^* Pe$, the L rolls are characterized by $\omega_c^* = k_c^* = 0$, whereas $(\partial\omega/\partial k)_c^* = Pe$ is the group velocity for both patterns. By taking into account the relation (14) together with the fact that $(\partial^2\omega/\partial k^2)_c^* = \mathrm{O}(1)$, a balance between all terms of (15) suggests that $(k - k_c^*) = \mathrm{O}(\varepsilon)$, $\omega - \omega_c^* = \mathrm{O}(\varepsilon^2)$ and $(\partial\omega/\partial k)_c^* = Pe = \mathrm{O}(\varepsilon)$. While the two first assumptions suggest that the modulation is at slow spatial and temporal scales, which are described by the coordinates

$$X = \varepsilon x \quad \text{and } \tau = \varepsilon^2 t \tag{16}$$

the assumption that $Pe = \mathrm{O}(\varepsilon)$ is a necessary condition to derive the coupled envelope equations in a consistent manner. Moreover, this assumption allows us to locate correctly the transition from convective to absolute instability as we will see later on and as it was pointed out by Carrière et al. [17] in their study of $P.R.B.$ problem. Otherwise if $Pe = \mathrm{O}(1)$ the scaling (16) is no longer valid and must be replaced by a long time scale $\tau = \varepsilon^2 t$ and a long spatial scale $\zeta = \varepsilon\ (x + Pe\ t)$ which is a slow, moving coordinate, travelling with the group velocity Pe.

After this clarification, the derivation of the coupled envelope equations is described below, assuming that $Pe = \varepsilon\,\widetilde{Pe}$ with $\widetilde{Pe} = \mathrm{O}(1)$ and that the amplitudes A and B appearing in (12), (13) are such that $A = A(X, \tau)$ and $B = B(X, \tau)$.

We expand the solution of (7) with respect to ε,

$$\mathbf{\Phi}(\mathbf{x}, \mathbf{y}, \mathbf{z}, \mathbf{t}, \mathbf{X}, \tau) = \varepsilon\mathbf{\Phi}_1 + \varepsilon^2\mathbf{\Phi}_2 + \varepsilon^3\mathbf{\Phi}_3 + \cdots \tag{17}$$

where the arguments of the left-hand side are repeated on the right-hand side. Substituting $\partial/\partial t \to \partial/\partial t + \varepsilon^2\partial/\partial\tau$, $\partial/\partial x \to \partial/\partial x + \varepsilon\partial/\partial X$, according to (16) and inserting (14) as well as $Pe = \varepsilon\,\widetilde{Pe}$ into (7) yields at successive orders of ε,

$$(I\partial/\partial t + L_0)\mathbf{\Phi}_1 = 0 \tag{18}$$

$$(I\partial/\partial t + L_0)\mathbf{\Phi}_2 = -L_1\mathbf{\Phi}_1 + N_2 \tag{19}$$

$$(I\partial/\partial t + L_0)\mathbf{\Phi}_3 = -L_1\mathbf{\Phi}_2 - L_2\mathbf{\Phi}_1 - I\partial/\partial\tau\,\mathbf{\Phi}_1 + N_3 \tag{20}$$

The explicit form of L_0, L_1, L_2, N_2 and N_3 is given in Appendix A.

For the sake of brevity, we formally describe the method of the derivation of coupled envelope equations and the reader should consult Ref. [22] for technical details. At the leading order the $\mathrm{O}(\varepsilon)$ equations are identical to the equations solved for the linear stability analysis [5,9]. The solution at this order is given in Appendix A. The right-hand side of Eq. (19) depends

only on $\mathbf{\Phi}_1$, which is already calculated at order ε. Therefore, Eq. (19) is an inhomogeneous boundary-value problem for $\mathbf{\Phi}_2$ that we have solved by integration. After inserting $\mathbf{\Phi}_1$ and $\mathbf{\Phi}_2$ into Eq. (20), there is no real need to solve this equation. Instead, by projecting this equation onto $\widehat{\mathbf{\Phi}_1}$, which is the solution to the adjoint problem (18), the right-hand side of Eq. (20) yields a solvability condition. By re-introducing the original variables $x = X/\varepsilon$, $t = \tau/\varepsilon^2$, $\widetilde{Pe} = Pe/\varepsilon$, $Ra_2 = (Ra - Ra^*)/\varepsilon^2$, $Re_2 = (Re_K - Re_K^*)/\varepsilon^2$ and re-defining $\varepsilon\mathbf{\Phi}_1$ as $\mathbf{\Phi}_1$ these solvability conditions are the coupled envelope equations for A and B,

$$\partial A/\partial t = -Pe\,\partial A/\partial x + \nu_A \partial^2 A/\partial x^2 + \gamma_0 A - \gamma_1 |A|^2 A - \gamma_2 |B|^2 A \tag{21}$$

$$\partial B/\partial t = -Pe\,\partial B/\partial x + \nu_B \partial^2 B/\partial x^2 + \lambda_0 B - \lambda_1 |B|^2 B - \lambda_2 |A|^2 B \tag{22}$$

where we have set: $\gamma_0 = \gamma_3(Ra - Ra^*)/Ra^* - \gamma_4(Re_K - Re_K^*)/Re_K^*$ and $\lambda_0 = \lambda_3(Ra - Ra^*)/Ra^* - \lambda_4(Re_K - Re_K^*)/Re_K^*$.

Each of these envelope equations features linear growth (term in $[\gamma_3(Ra - Ra^*)/Ra^* - \gamma_4(Re_K - Re_K^*)/Re_K^*]\ A$ in (21)), advection ($-Pe\,\partial A/\partial x$), diffusion ($\nu_A \partial^2 A/\partial x^2$), nonlinear saturation ($-\gamma_1|A|^2 A$) and nonlinear cross-saturation ($-\gamma_2|B|^2 A$), each term having a physical relevance.

The coefficients ν_A, ν_B, γ_i and λ_i ($i = 1, 2, 3, 4$) are functions of the lateral aspect ratio a and the Forchheimer number F. For porous media used in experiments [10–12], for which the aspect ratio is $a = 6.9$ and the values of F are very small ($O(10^{-4})$), we find that the bifurcation is supercritical (i.e. $\gamma_1 > 0$ and $\lambda_1 > 0$). In this case the computed coefficients are:

$$Ra^* = 39.53, \qquad Re_K^* = 0.19 * 10^{-2}, \qquad \gamma_1 = 0.323$$
$$\gamma_2 = 0.232, \qquad \gamma_3 = 0.5 * Ra^*, \qquad \gamma_4 = 22.13 * Re_K^*$$
$$\nu_A = 0.5, \qquad \nu_B = 0.025, \qquad \lambda_1 = 0.125, \qquad \lambda_2 = 0.472$$
$$\lambda_3 = 0.5 * Ra^*, \qquad \lambda_4 = 19.96 * Re_K^*$$

3.2. Nonlinear homogeneous states and their stability

Eqs. (21), (22) possess four homogeneous and stationary solutions,

(i) $A = B = 0$ for all γ_0 and λ_0 (conduction state).
(ii) $B = 0$, $A^2 = A_{3D}^2 = \gamma_0/\gamma_1$ with $\gamma_0 > 0$ (saturated T modes).
(iii) $A = 0$, $B^2 = B_L^2 = \lambda_0/\lambda_1$ with $\lambda_0 > 0$ (saturated L rolls).
(iv) $[A^2, B^2] = [A_m^2, B_m^2] = [(\gamma_2\lambda_0 - \gamma_0\lambda_1)/(\gamma_2\lambda_2 - \gamma_1\lambda_1); (\gamma_0\lambda_2 - \gamma_1\lambda_0)/(\gamma_2\lambda_2 - \gamma_1\lambda_1)]$ with $\gamma_2\lambda_0 - \gamma_0\lambda_1 > 0$ and $\gamma_0\lambda_2 - \gamma_1\lambda_0 > 0$ (mixed mode, i.e. existence of both homogeneous T modes and L rolls in the porous layer).

It is a straightforward matter to determine the stability of the various equilibrium solutions to small perturbations (see for example [16]). Here we focus on the results and we omit the detail.

(i) The conduction state is stable providing that $\gamma_0 < 0$ and $\lambda_0 < 0$.
(ii) The saturated T modes are stable if $\lambda_0 - \lambda_2\gamma_0/\gamma_1 < 0$ and unstable otherwise.
(iii) The saturated L rolls are stable if $\gamma_0 - \gamma_2\lambda_0/\lambda_1 < 0$ and unstable otherwise.
(iv) Since $\gamma_2\lambda_2 - \gamma_1\lambda_1 < 0$ the mixed mode is found to be unstable.

The results of the existence and the stability of the equilibrium solutions are qualitatively summarized in the parameter plane $((Re_K - Re_K^*)/Re_K^*; (Ra - Ra^*)/Ra^*)$ and are illustrated in Fig. 3. We also indicate the dynamic behavior leading to these equilibrium solutions in the $(A(t), B(t))$ space. Fig. 3 requires some comments:

In the region A_{3D} the only stable convective patterns are T modes. These modes become simultaneously stable with B_L rolls in the region B_L, A_{3D} meaning that the form of the bifurcated pattern depends on the initial conditions. In the region B_L the only stable convective patterns are L rolls. The mixed mode is unstable irrespective of the values of Re_K and Ra numbers. For $a = 6.9$ and $F \approx O(10^{-4})$, we find that the six straight lines of Fig. 3 are very close to the horizontal axis; therefore the region B_L, A_{3D} occupies nearly the whole upper half parameters plane of this figure.

3.3. Average heat transfer

The coupled envelope equations may be used to evaluate the Nusselt number measuring the total vertical heat transfer through the layer reduced by its conductive contribution. In the regions of parameter space where L rolls and/or T modes are stable, the mean Nusselt number N is defined [1] as

$$N = 1 + \langle w\theta \rangle \tag{23}$$

where $\langle w\theta \rangle$ has the meaning of average in space of the quantity $w\theta$ for L rolls, and its average in space as well as in time over a cycle for T modes.

Substituting the solutions for L rolls and for T modes at different orders after eliminating the slow space scale on the grounds presented in Section 3.1 yields the following relationships

$$N_L - 1 = \alpha_L \left\{ Ra/Ra_c^{\parallel}(Re_K, a) - 1 \right\} \quad \forall Ra \geqslant Ra_c^{\parallel} \tag{24}$$

$$N_{3D} - 1 = \alpha_{3D} \left\{ Ra/Ra_c^{3D}(Re_K, a) - 1 \right\} \quad \forall Ra \geqslant Ra_c^{3D} \tag{25}$$

where it is obvious that $N_L = 1$ and $N_{3D} = 1$ $\forall Ra < Ra_c^{\parallel}$ and $\forall Ra < Ra_c^{3D}$ respectively, indicating that the convection heat transfer branches off from the conductive heat transfer line at the critical value of the Rayleigh number. The slope for the Nusselt curve is $\alpha_L = 2$ for L rolls, while the slope α_{3D} for T modes depends on a as it is shown in Fig. 4.

For a fixed value of a, as relations (10), (11) show that for both L rolls and T modes, the critical Rayleigh number for convection is greater than the corresponding Rayleigh number without through-flow, it can be concluded that the presence of a through-flow has a retarding effect on heat transfer. This behavior is similar to that encountered in $P.R.B.$ problem as it

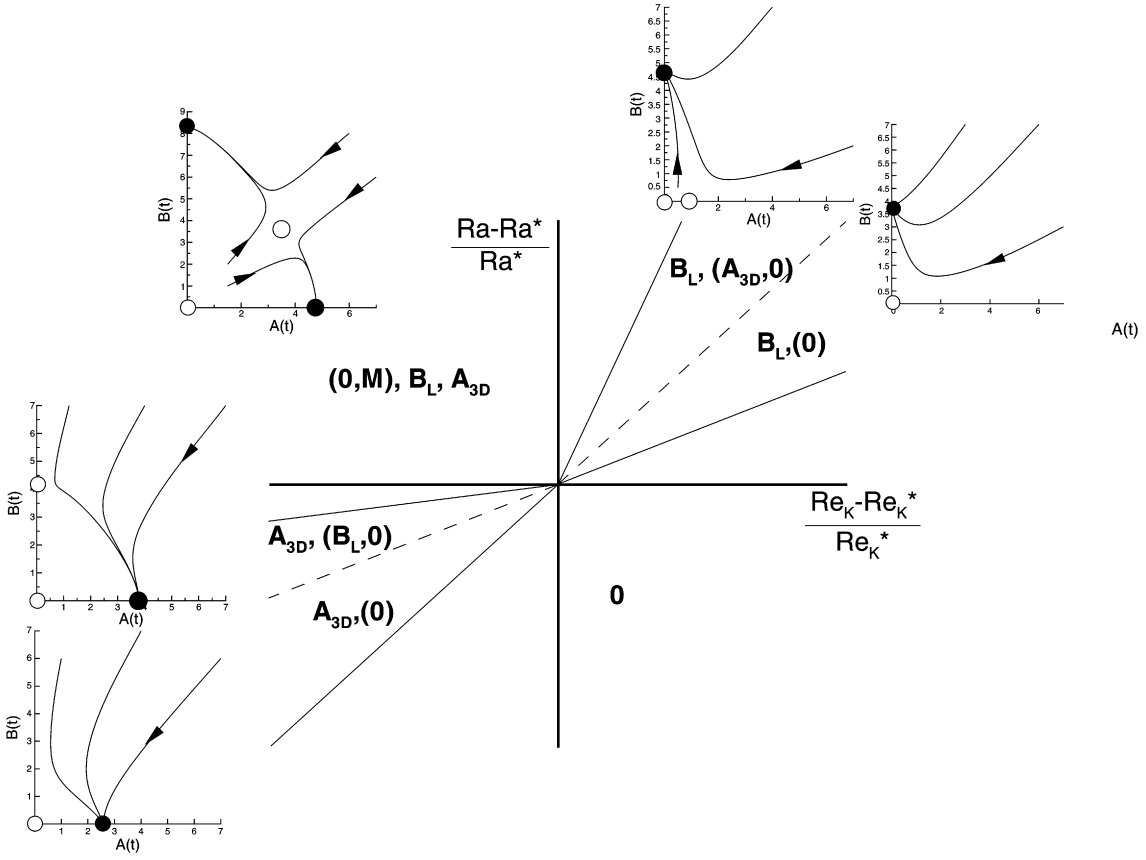

Fig. 3. Bifurcation diagrams in $(\frac{Re_K - Re_K^*}{Re_K^*}, \frac{Ra - Ra^*}{Ra^*})$ plane. 0 denotes the conduction state, A_{3D} denotes the transverse modes, B_L denotes the longitudinal rolls, and M denotes the mixed modes. A state without parentheses denotes a stable solution, whereas with parentheses it denotes an unstable solution. The succession of phase portraits for different regions is shown in the $(A(t), B(t))$ plane where the filled circle denotes the stable homogeneous solution and the empty circle denotes the unstable one.

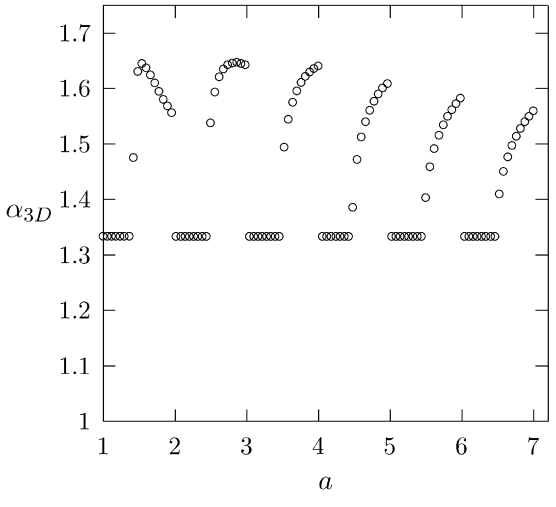

Fig. 4. Coefficient α_{3D} of the Nusselt number N_{3D} versus the aspect ratio a.

is reported by Nicolas (see [13] and references therein). Nevertheless, for porous media and for the average filtration velocity used in experiments [10–12]) we find that Re_K remains very small ($Re_K = O(10^{-3})$). The consequences of the weak Re_K dependence of $Ra_c^{\parallel}(Re_K)$ and $Ra_c^{3D}(Re_K)$ are that the average heat transfer is not significantly influenced by the presence of an horizontal through-flow. This prediction is in a qualitative good agreement with the experimental findings [10–12].

The variations of $Ra_c^{\parallel}(Re_K, a)/\ (1 + Re_K)$ in function of the lateral aspect ratio a, combined with the expression (24) suggest that for integer values of a, N_L is the same as that representing the mean heat transfer for infinite lateral aspect ratio. Otherwise the effect of the lateral confinement is to reduce the mean heat transfer. In $P.R.B.$ problem, among very rare investigations on the lateral confinement dependence of Nusselt number, Chen and Lavine [23] and Narusawa [24] performed numerical simulations of L rolls. While the numerical results of [23] concluded that a finite lateral aspect ratio raises the heat transfer, the converse is found in [24]. It can be concluded that as far as $P.R.B.$ problem is concerned, the influence of the lateral confinement on heat transfer is not completely understood.

Although mixed convection in porous media and $P.R.B.$ problem are qualitatively similar in a number of respects, the important differences may be explained by the effect of the solid matrix which plays a fundamentally important role in the determination of heat transfer. Indeed, in porous media the Nusselt number is not only a function of Rayleigh number but also depends on the solid-fluid combinations. In particular, it is well known that widely different conductivities of the solid and fluid phases cause local thermal nonequilibrium [25,26]. Much depends on other factors. If the microscopic length scale

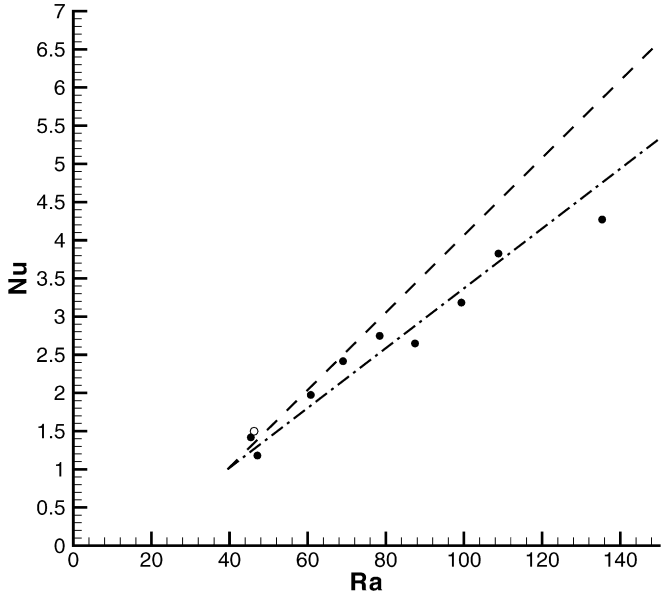

Fig. 5. *Nu* as a function of *Ra*: computed results from this study for L rolls ($--$) and for T modes ($- \cdot -$) and experimental results from Ref. [12] where the filled circle denotes T modes and the empty circle denotes L roll.

is very small indeed, then local thermal equilibrium is much more likely. Here we restrict the quantitative comparison with experiments to the case of water-glass combination for which the thermal conductivity of the porous matrix is close to that of the fluid. The heat transfer results corresponding to the experimentally observed T modes and L rolls (see Fig. 14 of [10] or Fig. 52 of [12]) together with theoretical predictions (24), (25) with $a = 6.9$ are displayed in Fig. 5. The *Nu* versus *Ra* plot of this figure indicates that up to $Ra \simeq 120$, the theoretical results of N_{3D} are in agreement with the measured Nusselt number corresponding to T modes. Concerning the predicted N_L, any serious conclusion can not be drawn because as it is shown in Fig. 5, we only dispose of one N_L experimental datum in the range of Rayleigh numbers we explore in this study (i.e. $Ra < 140$).

4. Pattern selection in the unstable region

In [9], we performed a spatio-temporal stability analysis and showed the relevance of the distinction between convective and absolute instability of both T modes and L rolls. Indeed, comparison with early experiments [10–12]) indicates that the theoretical transition curve from convective to absolute instability in the Rayleigh–Péclet number plane corresponds perfectly to the observed transition from moving T modes to stationary L rolls and vice versa. Although this result is very important, the concept of absolute instability can not explain the experimentally observed L rolls in the convectively unstable parameters (i.e. region below the curve of Fig. 1). This section aims at characterizing flow patterns that can arise from amplification of permanent source of perturbations. This permanent source may be thought of as describing unavoidable inlet disturbances and thermal or other noise sources in laboratory experiments.

4.1. Absolute versus convective instability of the conductive state

It is straightforward to calculate the boundary for absolute instability within the context of envelope equations (21), (22). Consider a small spatially localized perturbation of the conductive state (5). Under the linear part of envelope equations (21), (22), the amplitude evolution of T modes and L rolls is dominated by the exponential factor [27]

$$(G_A, G_B) = 1/(4\pi t)^{1/2} \times (\mathrm{e}^{(\gamma_0-(x/t-Pe)^2/4\nu_A)t}, \mathrm{e}^{(\lambda_0-(x/t-Pe)^2/4\nu_B)t}) \tag{26}$$

The ray along which the maximum growth rate is reached is defined by $x/t = Pe$. Thus, for $\gamma_0 = 0$ and $\lambda_0 = 0$ we reobtain the convective threshold for T modes and L rolls respectively. The condition for the onset of absolute instability can be found by vanishing the growth rate for a given x as $t \to \infty$, that is $x/t \to 0$. This yields:

$$\gamma_0 = Pe^2/4\nu_A \quad \text{and} \quad \lambda_0 = Pe^2/4\nu_B \tag{27}$$

The absolute instability boundary for T modes and for L rolls is then obtained by substituting γ_0, λ_0, ν_A and ν_B by their expressions in functions of dimensionless parameters *Ra*, *Pe*, the lateral aspect ratio a and the Forchheimer number F. For $a = 6.9$ and $F = 10^{-4}$ these boundaries are plotted in the (*Pe*, *Ra*) plane of Fig. 6 as a dashed line for T modes and a dotted-dashed line

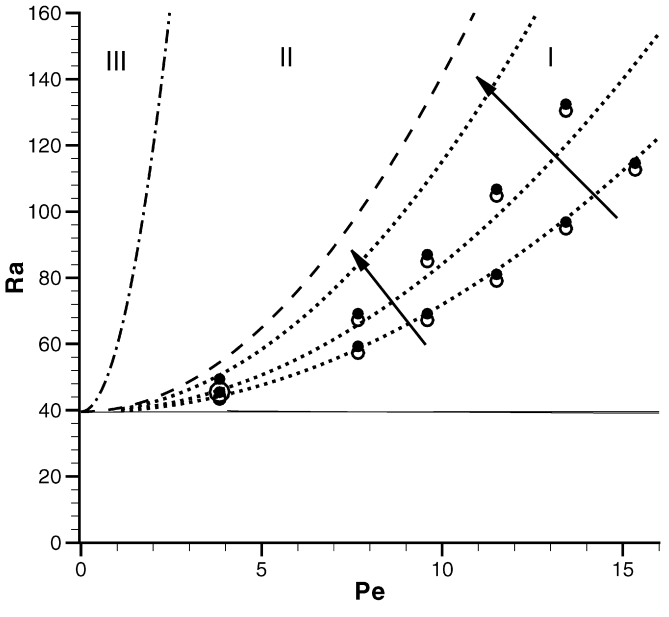

Fig. 6. Stability curves in the (*Pe*, *Ra*) plane. The conductive state is convectively unstable with respect to both T modes and L rolls in the region I below the dashed line. It becomes absolutely unstable with respect to T modes in the region II. The dotted-dashed line separates the region II from the region III, where the basic state is absolutely unstable with respect to both two-patterns. The dotted lines in the region I represent the L rolls/T modes transition as it is predicted by the linear criterion (35) in presence of inlet forcing (36) with $\alpha = 0.001, \alpha = 0.01$ and $\alpha = 0.1$. The arrows indicate how these transition curves move when α is increased. The combined symbols ($\circ\bullet$) represent the L rolls/T modes transition as it was found by numerical simulations of the coupled envelope Eqs. (21)–(22) with $\alpha = 0.001$ and $\alpha = 0.01$.

for L rolls. The absolute instability boundary for T modes was compared to the one that was determined from the full dispersion equation of the problem in [9]. We found that the results stemming from the envelope equation approximations are valid in the whole range of moderate Péclet numbers (i.e. $Pe < 5$) and the accuracy is excellent for small ones.

4.2. Spatial amplification in the convectively unstable region

In the first part of this subsection, we use the linear versions of envelope equations (21), (22) to characterize the spatial amplification of perturbations in the convectively unstable parameter region defined by $\gamma_0 < Pe^2/4\nu_A$ and $\lambda_0 < Pe^2/4\nu_B$ (i.e. region I of Fig. 6). Following Deissler [28], the amplitudes can be expanded as

$$\big[A(x,t),\, B(x,t)\big] = \int_{-\infty}^{+\infty} \big[A_0(\omega),\, B_0(\omega)\big] \mathrm{e}^{-\mathrm{i}(kx+\omega t)} \mathrm{d}\omega \tag{28}$$

where the frequency ω is real and the wave number $k = k_r + \mathrm{i}k_i$ is complex. Here $A_0(\omega)$ and $B_0(\omega)$ represent Fourier transforms of some persistent, however small, perturbations $A(x = 0, t)$ and $B(x = 0, t)$ of the flow at the entrance cross-section of the porous medium. These inlet perturbations may be amplified further downstream with a spatial amplification described by k_i. If we insert (28) into the linear parts of (21), (22) we obtain the dispersion relation which can be written, for example for A, in the spatial form $k^A(\omega)$,

$$k^A(\omega) = \mathrm{i}(Pe - \sqrt{Pe^2 - 4\nu_A(\gamma_0 + \mathrm{i}\omega)})/2\nu_A \tag{29}$$

If the dimensionless parameters of the problem allow a spatial growth (i.e. $k_i > 0$), a band of frequencies ω with $\omega_- < \omega < \omega_+$ may be amplified. The limits $\omega_\pm$ of this band are found by imposing $k_i = 0$ and read

$$\omega_\pm = \pm Pe\sqrt{\gamma_0/\nu_A} \quad \text{for } A \quad \text{and}$$
$$\omega_\pm = \pm Pe\sqrt{\lambda_0/\nu_B} \quad \text{for } B \tag{30}$$

The frequency ω_M which gives the maximum spatial growth rate is found from $\partial k_i/\partial\omega = 0$, giving

$$\omega_M = 0 \quad \text{and} \quad k_r = 0 \tag{31}$$

The corresponding maximum spatial growth rate is

$$k_i^A = \big(Pe - \sqrt{Pe^2 - 4\gamma_0\nu_A}\big)/2\nu_A \quad \text{for } A \quad \text{and}$$
$$k_i^B = \big(Pe - \sqrt{Pe^2 - 4\lambda_0\nu_B}\big)/2\nu_B \quad \text{for } B \tag{32}$$

It is important to note that the spatial growth rate is defined only if $Pe^2 - 4\gamma_0\nu_A > 0$ for A and $Pe^2 - 4\lambda_0\nu_B > 0$ for B. These conditions are not satisfied in the absolutely unstable parameter region meaning that this spatial approach is not valid when the instability becomes absolute.

We now turn to the fundamental question related to the prediction of the onset of either T modes or L rolls in the parameter range where both patterns are convectively unstable. According to (31) and (32) T modes envelope and L rolls envelope with the maximum spatial growth rate take the form $[A(x), B(x)] = [A_0(\omega_M = 0)\ \mathrm{e}^{k_i^A x},\ B_0(\omega_M = 0)\ \mathrm{e}^{k_i^B x}]$. Let us define an entrance length x_h as the distance from the inlet cross section to a spatial position at which nonlinear terms begin to saturate the spatial growth. More precisely, we suppose that L rolls amplitude reaches the half of its saturated amplitude B_L at x_h

$$B_0\mathrm{e}^{k_i^B x_h} = B_L/2 \tag{33}$$

The condition that must be fulfilled if we assume that L rolls dominate over T modes at the spatial location x_h (i.e. $B_0\mathrm{e}^{k_i^B x_h} > A_0\mathrm{e}^{k_i^A x_h}$) reads

$$(1/x_h)\ln(B_0/A_0) > k_i^A - k_i^B \tag{34}$$

Substituting the expression of x_h from (33) into the inequality (34) yields

$$\ln(B_0/A_0)/\ln(B_L/2B_0) > (k_i^A/k_i^B) - 1 \tag{35}$$

Note that if $B_0 = A_0$, the condition (35) is reduced to $k_i^B > k_i^A$. We emphasize that there is no information available about the experimental perturbation intensity in [10–12]. Moreover, it is not even clear that the inlet perturbation A_0 for T modes and B_0 for L rolls should be of the same order of magnitude. Therefore we consider the more general case where the quantities k_i^A, k_i^B, B_0 and A_0 act in concert in the selection process. In the following, let us assume that A_0 and B_0 are related to saturated amplitudes of T modes and L rolls as:

$$A_0 = \alpha A_{3\mathrm{D}} \quad \text{and} \quad B_0 = \alpha B_L \tag{36}$$

and illustrate the selection process in the (Pe, Ra) plane as it is predicted by the criterion (35) for different values of small α. This task is achieved by using expressions (32) to calculate k_i^A/k_i^B for varying values of Pe and Ra. Fig. 6 displays the results for $\alpha = 0.001$, 0.01 and 0.1. For a fixed value of α, and below the corresponding dotted curve of this figure where the condition (35) is satisfied, L rolls are expected to dominate over T modes, while the converse occurred above this curve. We also note that as soon as α is augmented gradually, the curve describing a L roll/T mode transition approaches the border between convective and absolute instability.

All these predictions are associated with linear properties in the sense that both amplitudes $A(x)$ and $B(x)$ must be small. As a consequence, this linearized picture is expected to be valid at the best up to only $x = x_h$, a spatial position at which nonlinear effects begin to be non-negligible. As the downstream position x becomes larger than x_h, a nonlinear spatial analysis is required to clarify which pattern may be selected. This task will be achieved in two ways. We first assume that at large x, L rolls have reached their saturated amplitude $B_L = \sqrt{\lambda_0/\lambda_1}$. Therefore, using the nonlinear equation (21) we determine the spatial growth $k_i^{A,B}$ associated with the most amplified T modes according to linear theory (i.e. mode with $\omega_M = 0$) in presence of saturated L rolls. Similarly, Eq. (22) allows us to calculate the maximum spatial growth $k_i^{B,A}$ of L rolls in presence of saturated amplitude $A_{3\mathrm{D}} = \sqrt{\gamma_0/\gamma_1}$ of T modes. After some calculations one gets

$$k_i^{A,B} = \big(Pe - \sqrt{Pe^2 - 4\nu_A(\gamma_0 - \gamma_2\lambda_0/\lambda_1)}\big)/2\nu_A \quad \text{for } A \tag{37}$$

and

$$k_i^{B,A} = \left(Pe - \sqrt{Pe^2 - 4\nu_B(\lambda_0 - \lambda_2\gamma_0/\gamma_1)}\right)/2\nu_B \quad \text{for } B \quad (38)$$

Eq. (37) states that $k_i^{A,B} < 0$ provide that $\gamma_0 - \gamma_2\lambda_0/\lambda_1 < 0$ meaning that T modes are spatially damped in the space region where saturated L rolls are well developed. Similarly, according to Eq. (38) L rolls can not experience any spatial growth in presence of uniform T modes if $\lambda_0 - \lambda_2\gamma_0/\gamma_1 < 0$. Moreover for $a = 6.9$ and $F \approx \mathrm{O}(10^{-4})$, inequalities $\gamma_0 - \gamma_2\lambda_0/\lambda_1 < 0$ and $\lambda_0 - \lambda_2\gamma_0/\gamma_1 < 0$ hold for almost all combinations of *Pe–Ra* numbers. Consequently, homogeneous T modes and L rolls can not develop at the same spatial location. These results stemming from the nonlinear spatial stability approach are consistent with the nonlinear temporal stability analysis performed in Section 3.1 which concluded that the mixed mode is an unstable thermo-convective configuration.

5. Numerical results

In this section we describe results of numerical simulations of the coupled envelope equations (21), (22) above threshold, since they allow to investigate the validity of the above analytical findings as well as to understand some experimental results. In fact, the difficulty to handle mathematically the nonlinear original theoretical model (1) leading to the lack of analytical results makes relevant the use of coupled envelope equations. Furthermore, it has often been checked that their validity qualitatively extends far beyond the instability threshold. The numerical experiments provide a test of the following predictions:

(i) that in the convectively unstable parameter region (region *I* of Fig. 6), the nonlinear development of L rolls or T modes depends on the magnitude of the inlet forcing, and that the location of L roll/T mode transition is ruled by the linear criterion (35);
(ii) that coexisting convective states with saturated amplitudes of L rolls and T modes at the same spatial location are unstable solutions;
(iii) that the dominant patterns are T modes in the *Pe–Ra* parameter region where these modes are absolutely unstable, whereas L rolls still convectively unstable (region *II* of Fig. 6).

In addition, we also investigate the selection process in the region *III* of Fig. 6 where both T modes and L rolls are absolutely unstable.

To integrate the coupled envelope equations (21), (22) we use a Crank–Nicholson (semi-implicit) discretization in time whereas the spatial derivatives are discretized by centered, symmetric second-order formulas. As it is well known, the Crank–Nicholson scheme is always numerically stable when the solution is physically stable. However, Cossu and Loiseleux [29] showed that when the solution becomes physically unstable, a Crank–Nicholson scheme with a spatial grid size of Δx and a time resolution of Δt may experience a numerical transition from absolute to convective instability and vice versa. In the framework of the Landau–Ginzburg equation, these authors derived conditions on the discretization parameters Δx and Δt in order to avoid such numerical transition. Therefore, our numerical experiments are performed with Δx sufficiently small in order to respect the criterium derived in [29]. The length of the porous medium is imposed to be 50. The outlet boundary conditions are chosen so that the amplitudes A and B are assumed to be equal to their saturated values,

$$A(x + \mathrm{d}x, t + \mathrm{d}t)/A(x,t) = A(x,t)/A(x - \mathrm{d}x, t - \mathrm{d}t)$$
$$B(x + \mathrm{d}x, t + \mathrm{d}t)/B(x,t) = B(x,t)/B(x - \mathrm{d}x, t - \mathrm{d}t) \quad (39)$$

5.1. Simulations in the convectively unstable region

In the *Pe–Ra* parameter space where both L rolls and T modes are convectively unstable (i.e. region *I* of Fig. 6), we performed numerical simulations in the absence of any inlet forcing with two different initial conditions: in the first case, both the amplitude A for T modes and the amplitude B for L rolls were initialized by a localized spatial Gaussian function; in the second case, we started from a randomly distributed perturbation of A and B.

Both the initial conditions gave rise to the growth of wave packets which migrated downstream with time, leaving the flow domain unperturbed, as shown in Fig. 7. These results suggest that it is necessary to revisit the interpretation of experimental observations [10–12]) concerning the formation and development of L rolls in the convectively unstable region. In fact, the convective nature of the instability mechanism implies that the L rolls actually observed in the laboratory may arise from spatial amplification of some persistent perturbations of the flow. Although the actual perturbation source may be spatially distributed, one may picture it at the entrance cross-section of the channel. This picture is conceptually useful because the perturbation furthest upstream has the most time to grow before reaching a given axial position. Various questions then arise.

Does the forced development of L rolls eventually lead to the establishment of an equilibrium amplitude B_L? Is such an equilibrium amplitude dependent on the magnitude of the forced perturbations at the entrance cross-section? More important, how does the selection of L rolls rather than T modes depend on the inlet forcing?

Answering these questions may be pursued through a series of suitable numerical experiments with an imposed inlet forcing. Here, the strength of the inlet forcing is simply connected to saturated amplitudes $A_{3\mathrm{D}}$ and B_L by (36).

In order to avoid any repetition in the next subsection, we report in Fig. 8 the whole results obtained by numerous numerical tests, not only in the region *I*, but also in the regions *II* and *III* of Fig. 6. Specifically, for parameter range where the instability is convective, Fig. 8 demonstrates that the region *I* is divided in two parts; in one part L rolls (○) are dominant, while in the other part T modes (●) win the competition between the two types of patterns. Furthermore, we have checked the relevance of the linear criterion (35) to represent the numerical L roll/T mode transition. Fig. 6 displays the numerical results corresponding

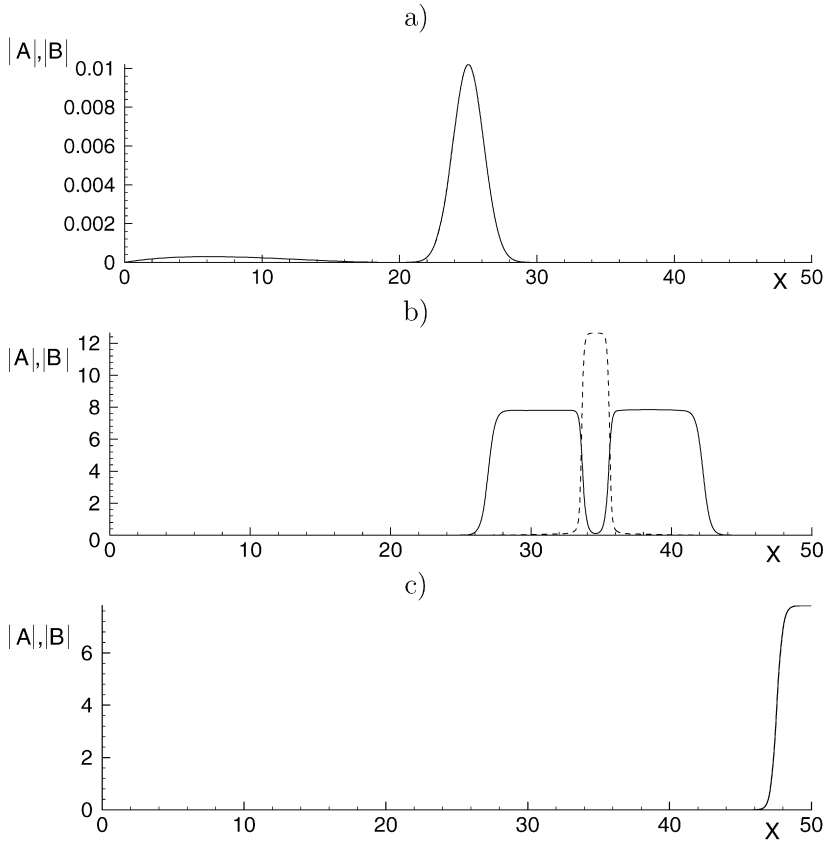

Fig. 7. Transient behavior of the envelope $|A|$ for T modes (−) and $|B|$ for L rolls (−−) in convective unstable regime at $t = 1$ (b) and $t = 7.4$ (c) generated by a Gaussian profile of $|A|$ and $|B|$ (a). The expansion of wavepackets in the down-stream direction is clear from this figure. Parameters are $Pe = 9.6$ and $Ra = 79$.

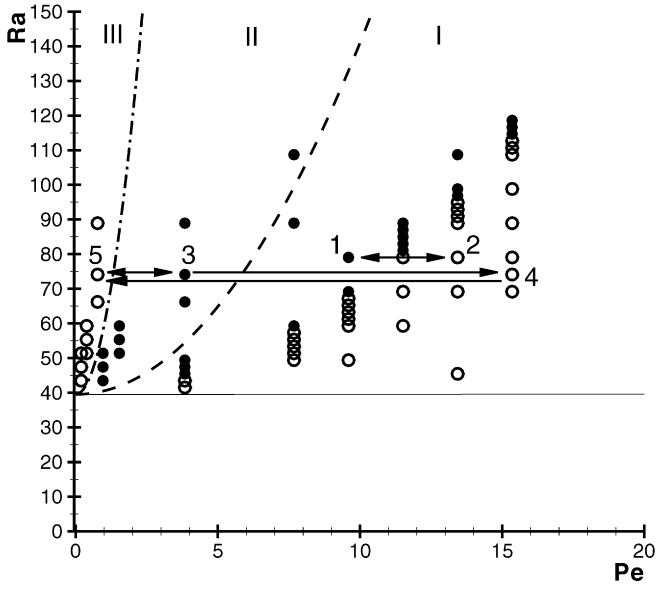

Fig. 8. Flow regime map for patterns obtained by numerical simulations of coupled envelope equations (21), (22) in the three regions of the (Pe, Ra) plane: T modes (•) and L rolls (○).

to two inlet perturbations (36) with $\alpha = 0.001$ and $\alpha = 0.01$ respectively. Quite remarkably, this figure demonstrates that the analytical linear criterion (35) perfectly captures the numerical transition from L rolls to T modes and vice versa.

In order to exemplify the competition between L rolls and T modes, we present the results of numerical tests corresponding to an increase or to a decrease of the flow rate Pe, keeping the porous thermal Rayleigh number Ra constant. The first simulation is carried out with $Ra = 79$ and $Pe = 9.62$ (point 1 in Fig. 8) in presence of inlet forcing (36) with $\alpha = 0.001$ and starting with small random perturbations for A and B. Fig. 9(a) shows that the linear spatial growth rate of A overwhelms that of B near the entrance channel so that T modes develop down-stream while L rolls are damped. The results obtained from this run were used as initial conditions for the next run performed with increasing Péclet number to $Pe = 13.46$ keeping $Ra = 79$ (point 2 in Fig. 8). Nonlinear competition between L rolls and T modes is displayed in Fig. 9(b) for a transient state which shows the coexistence of these two types of patterns in different areas of the channel; L rolls occupy the part near the inlet while T modes are well developed in the second part of the medium. This result is consistent with experimental observations [12]. When time grows progressively, the front separating L rolls from T modes travels in the down-stream direction with a velocity equals to Pe and eventually reaches the outlet of the channel. The resulting long-time patterns are saturated L rolls (Fig. 9(c)). Starting a run from these developed L rolls with the same Rayleigh number and returning to $Pe = 9.62$ we recover T modes (Fig. 9(d)), meaning that the transition process does not experience any hysteresis effect. In addition, numerical solutions presented in Fig. 9(a,c,d) show that when one type of

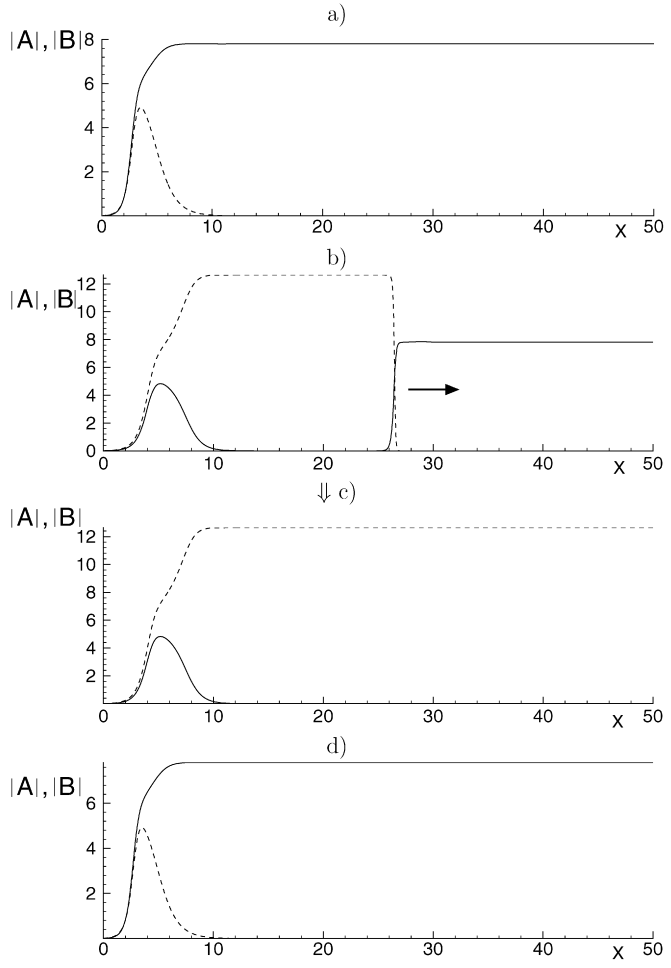

Fig. 9. Envelope $|A|$ for T modes $(-)$ and $|B|$ for L rolls $(--)$ as a function of the spatial coordinate x in the convectively unstable parameters. The Rayleigh number is kept constant at $Ra = 79$, while the Péclet number increases from $Pe = 9.62$ (a) to $Pe = 13.46$ (b, c) and returns to its initial value $Pe = 9.62$ (d). These parameters are associated to points 1 and 2 of Fig. 8. The numerical tests are performed in presence of inlet forcing (36) with $\alpha = 0.1\%$.

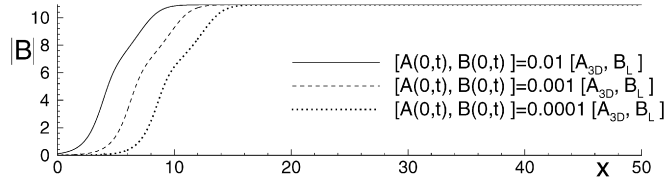

Fig. 10. Envelope $|B|$ of L rolls with $Ra = 69.18$ and $Pe = 15.34$ for different level of inlet noise for $A(x,t)$ and $B(x,t)$.

patterns reaches its saturated amplitude, the other pattern is spatially damped. This result confirms our analytical predictions that mixed mode, i.e. coexisting saturated L rolls and saturated T modes at the same spatial location, is an unstable solution.

We emphasize that in all performed simulations in the convectively unstable region, the amplitude of saturated L rolls is found to be independent of the magnitude of the inlet perturbation. This is shown in Fig. 10 where three different responses to inlet forcing are reported. Note that the smaller the magnitude of the inlet perturbation, the farther the cross-section where the amplitude saturation is achieved.

5.2. Simulations in the absolutely unstable region

The second numerical runs are devoted to characterize patterns that dominate in the *Pe–Ra* parameter space where the basic state is absolutely unstable to T modes (regions *II* and *III* of Fig. 6). The flow structures observed in our numerical experiments are previously summarized by the flow regime map shown in Fig. 8. This figure shows that a nonlinear development of T modes occurs in the region *II* as it is expected. The most striking result is that parameters of region *III* promote the development of L rolls, although, at the linear level, the basic state is also absolutely unstable with respect to T modes. We believe that the nonlinear cross-coupling between the amplitudes A and B may explain this selection process, which is found to be independent both of initial conditions and of the level of the inlet perturbation. Additionally, it is found that the T mode/L roll transition can be well characterized by the curve of absolute instability of the basic state with respect to L rolls (i.e. the curve separating regions *II* and *III* of Fig. 6).

Selected results from numerical runs are presented in the following to illustrate the competition between T modes and L rolls and to test that L rolls that appear in region *III* of Fig. 6 are not sustained by a finite entrance forcing. Starting from a localized disturbance at $Ra = 79$ and $Pe = 0.77$, the spatio-temporal evolution of the T modes and the L rolls envelopes $|A|$ and $|B|$ is described in Fig. 11. For small and intermediate values of time (Fig. 11(b,c)), two transient wave-packets of T modes develop, travelling in opposite directions; a wave-packet of L rolls is seen to be sandwiched between them. As time grows, a new L rolls front is created near the entrance cross-section and invades into T modes state (Fig. 11(d)). The resulting long-time pattern is a self-sustained L rolls structure (Fig. 11(e)).

Finally, we have examined qualitatively some further successive transitions of flow patterns observed in experiments, namely the transitions from point 34 to point 35 and then to point 36 of the flow regime map of Fig. 1 or the transition from point 38 to point 39 of the same figure. In order to mimic these experimental transitions which occur for $Ra \approx 130$ and $2 < Pe < 40$, numerical tests are performed by fixing Rayleigh number at $Ra = 75$ and adjusting Pe to its value for points 3 ($Pe = 4$), 4 ($Pe = 16$) and 5 ($Pe = 1$) of Fig. 8. The numerical experiment is started from the saturated developed T modes (point 3 of Fig. 8) in the presence of a forcing perturbation (36) at the entrance cross section with $\alpha = 0.001$. Increasing Pe to reach the point 4 of Fig. 8, after transient states, T modes pattern is substituted by a fully developed L rolls pattern. If we suddenly decrease Pe to reach the point 5 of Fig. 8, L rolls structure remains the dominant mode. By ramping Pe forth and back between points 5 and 3 of Fig. 8, we verified that the transition between L rolls and T modes is free of a hysteresis.

6. Conclusion

In this paper we have studied the nonlinear behavior of mixed convection generated by both a unidirectional uniform flow and a vertical temperature gradient in a rectangular long porous medium. The mathematical model based on the Forch-

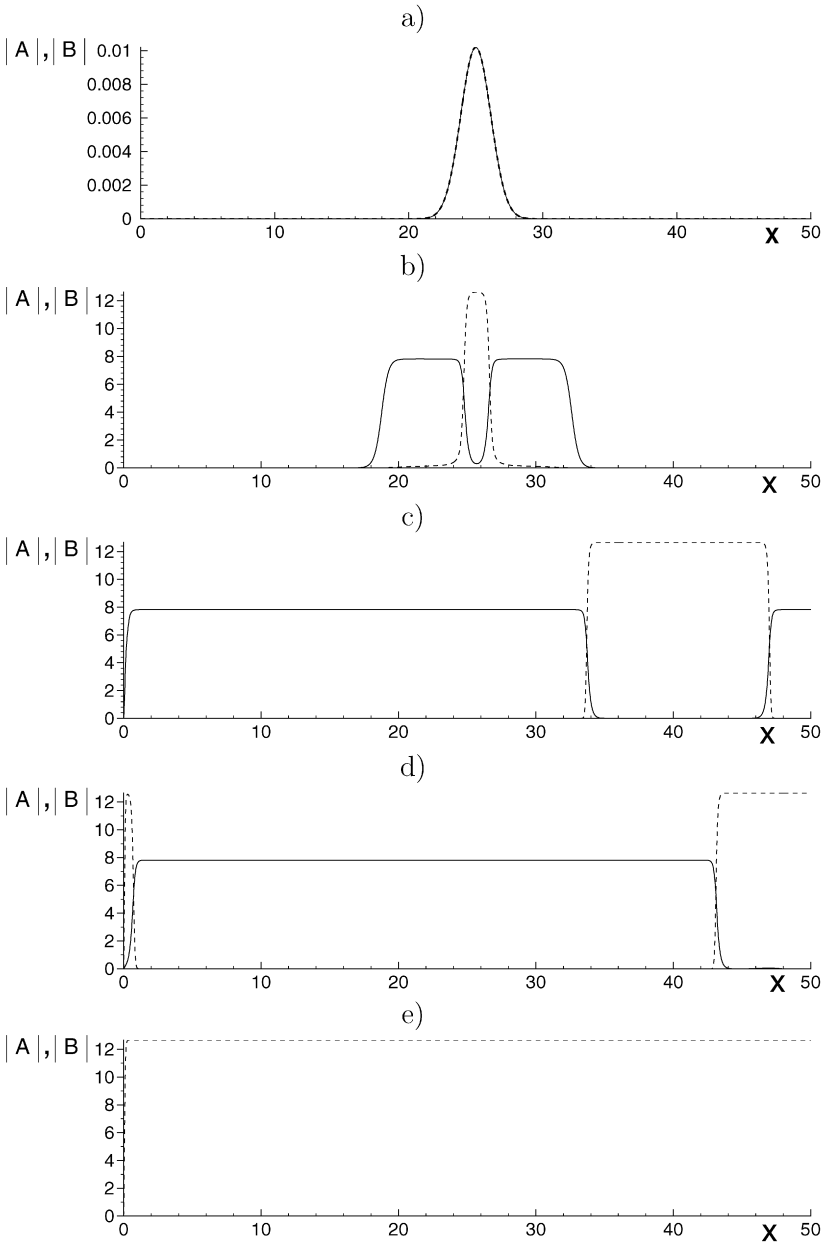

Fig. 11. Spatio-temporal evolution for four selected times, $t = 0.9$ (b), $t = 20$ (c), $t = 40$ (d), $t = 100$ (e) of the envelope $|A|$ for T modes $(-)$ and $|B|$ for L rolls $(--)$ built from localized Gaussian initial conditions (a). The parameters are $Ra = 79$ and $Pe = 0.77$.

heimer correction to Darcy's law allows for a basic state, which for sufficiently large Rayleigh number Ra turned out to be unstable. A perturbation analysis of the basic state showed in linear theory that convection started to develop in the form of either moving three-dimensional modes (T modes) if Reynolds number Re_K is below a critical value Re_K^* or in the form of stationary longitudinal rolls (L rolls) otherwise. A weakly nonlinear theory , which is valid near the double bifurcation point (Re_K^*, Ra^*), has been applied in order to derive coupled envelope equations for the marginally unstable T modes and L rolls. The procedure is similar to that presented by Kato and Fujimura [16], who obtained a coupled Landau equations describing the long-time behavior of the competition between T modes and L rolls in the Poiseuille–Rayleigh–Bénard problem. However, the situation near critical conditions is such, that a narrow spectrum of waves become unstable. Taking that into account, we obtained coupled envelope equations describing not only the temporal modulations of the envelope amplitudes of T modes and L rolls but also their modulations on a long spatial scale. The coupled envelope equations allow us to classify all the possible equilibrium solutions and their respective stability and to obtain a typical bifurcation diagram in which mixed mode composed of the two convective configurations is always unstable. The evaluated average heat transfer is found to decrease with increasing the magnitude of the imposed horizontal flow. Nevertheless, for weak values of Re_K, it is found in agreement with early experimental measurements [12], that the average heat transfer is not significantly influenced by the presence of

an horizontal through-flow. Moreover, quantitative comparisons demonstrate that up to three times the critical Rayleigh number, the predicted Nusselt number compares well with experimental data obtained with a water–glass combination [12].

The absolute and convective instability boundaries are determined for the two kinds of competing patterns. Numerical simulations of the coupled envelope equations with the conduction state imposed at the inlet of the porous medium reveal that no pattern may be sustained in the convectively unstable region. This, however, is an idealized result which is in contradiction with actual experimental observations of well developed L rolls. We therefore examine how these unsatisfactory predictions are modified in the presence of some permanent disturbances located at the entrance cross-section of the channel. Numerical simulations of coupled envelope equations demonstrated that the nonlinear development of such perturbations is shown to lead to either T modes or L rolls depending on the magnitude of the inlet disturbances. Quite remarkably, numerical results confirm that the observability of either of the two patterns is ruled by an analytical criterion we derived in this paper. In the *Pe–Ra* parameter space where the basic state is absolutely unstable, it is found that the T mode/L roll transition observed in laboratory experiments, is well characterized by the boundaries of absolute instability of the basic state with respect to L rolls. In addition, the numerical solutions show that the mixed mode, composed with the two types of pattern at the same spatial location is an unstable mode, confirming the analytical predictions.

Appendix A

Under the assumption of weak perturbations, the term $F\|\vec{V}\|$ associated to Forchheimer's correction reads:

$$F\|\vec{V}\| = Re_K + Fu + \frac{1}{2}\frac{F^2}{Re_K}(v^2+w^2) - \frac{1}{2}\frac{F^3}{Re_K^2}u(v^2+w^2) + \text{h.o.t.}$$

where h.o.t. stands for higher order terms

The operators I and L of Eq. (7) are defined by

$$I = \begin{bmatrix} 0 & 0 & 0 & 0 & 0 \\ 0 & 0 & 0 & 0 & 0 \\ 0 & 0 & 0 & 0 & 0 \\ 0 & 0 & 0 & 1 & 0 \\ 0 & 0 & 0 & 0 & 0 \end{bmatrix}$$

$$L = \begin{bmatrix} 1+2Re_K & 0 & 0 & 0 & \partial_x \\ 0 & 1+Re_K & 0 & 0 & \partial_y \\ 0 & 0 & 1+Re_K & -Ra & \partial_z \\ 0 & 0 & -1 & \nabla^2 & 0 \\ \partial_x & \partial_y & \partial_z & 0 & 0 \end{bmatrix}$$

The nonlinear part N of Eq. (7) is as follows:

$$N(\Phi,\Phi) = \begin{bmatrix} -Fu^2 - \frac{1}{2}F(v^2+w^2) \\ -Fuv - \frac{1}{2}\frac{F^2}{Re_K}v(v^2+w^2) \\ -Fuw - \frac{1}{2}\frac{F^2}{Re_K}w(v^2+w^2) \\ -\vec{v}.\nabla\theta \\ 0 \end{bmatrix}$$

L_0 is the linear operator L evaluated at the double bifurcation point (Re_K^*, Ra^*).

At $O(\varepsilon)$ we find that the eigenfunctions Φ_1 are

$$\Phi_1 = \begin{bmatrix} u_{1,1}e^{i(k_c^*x-\omega_c^*t)}\cos(\pi z)\cos(ly) \\ v_{1,1}e^{i(k_c^*x-\omega_c^*t)}\cos(\pi z)\sin(ly) \\ w_{1,1}e^{i(k_c^*x-\omega_c^*t)}\sin(\pi z)\cos(ly) \\ T_{1,1}e^{i(k_c^*x-\omega_c^*t)}\sin(\pi z)\cos(ly) \\ P_{1,1}e^{i(k_c^*x-\omega_c^*t)}\cos(\pi z)\cos(ly) \end{bmatrix} + \begin{bmatrix} u_{1,2}\cos(\pi z)\cos(l_0 y) \\ v_{1,2}\cos(\pi z)\sin(l_0 y) \\ w_{1,2}\sin(\pi z)\cos(l_0 y) \\ T_{1,2}\sin(\pi z)\cos(l_0 y) \\ P_{1,2}\cos(\pi z)\cos(l_0 y) \end{bmatrix} + \text{C.C.}$$

with $l = \pi m_{3D}/a$, $l_0 = \pi m_{\parallel}/a$ and

$$\begin{cases} u_{1,1} = \frac{ik_c^* A(X,\tau)\pi(1+Re_K^*)}{(2Re_K^*+1)l^2+(k_c^*)^2(1+Re_K^*)} \\ v_{1,1} = -\frac{A(X,\tau)\pi l(2Re_K^*+1)}{(2Re_K^*+1)l^2+(k_c^*)^2(1+Re_K^*)} \\ w_{1,1} = A(X,\tau) \\ T_{1,1} = \frac{A(X,\tau)}{\pi^2+l^2+(k_c^*)^2} \\ P_{1,1} = -\frac{A(X,\tau)\pi(1+Re_K^*)(2Re_K^*+1)}{(2Re_K^*+1)l^2+(k_c^*)^2(1+Re_K^*)} \end{cases}$$

$$\begin{cases} u_{1,2} = 0 \\ v_{1,2} = -\frac{B(X,\tau)\pi}{2l_0} \\ w_{1,2} = \frac{B(X,\tau)}{2} \\ T_{1,2} = \frac{B(X,\tau)}{2(\pi^2+l_0^2)} \\ P_{1,2} = -\frac{B(X,\tau)\pi(1+F\,Pe^*)}{2l_0^2} \end{cases}$$

At $O(\varepsilon^2)$, the operator L_1 and the nonlinear part N_2 are as follows

$$L_1 = \begin{bmatrix} 0 & 0 & 0 & 0 & \partial_X \\ 0 & 0 & 0 & 0 & 0 \\ 0 & 0 & 0 & 0 & 0 \\ 0 & 0 & 0 & \widetilde{Pe}\partial_x - 2\partial_{X,x}^2 & 0 \\ \partial_X & 0 & 0 & 0 & 0 \end{bmatrix}$$

$$N_2 = \begin{bmatrix} -Fu_1^2 - \frac{1}{2}F(v_1^2+w_1^2) \\ -Fu_1v_1 \\ -Fu_1w_1 \\ -\vec{v}_1.\nabla\theta_1 \\ 0 \end{bmatrix}$$

At $O(\varepsilon^3)$, the expressions of the operator L_2 and the nonlinear part N_3 are

$$L_2 = \begin{bmatrix} 2Re_2 & 0 & 0 & 0 & 0 \\ 0 & Re_2 & 0 & 0 & 0 \\ 0 & 0 & Re_2 & -Ra_2 & 0 \\ 0 & 0 & 0 & -\partial_X^2 + \widetilde{Pe}\partial_X & 0 \\ 0 & 0 & 0 & 0 & 0 \end{bmatrix}$$

$$N_3 = \begin{bmatrix} -2Fu_1u_2 - F(v_1v_2 + w_1w_2) \\ -F(v_1u_2 + v_2u_1) - \frac{1}{2}\frac{F^2}{Re_K}v_1(v_1^2 + w_1^2) \\ -F(w_1u_2 + w_2u_1) - \frac{1}{2}\frac{F^2}{Re_K}w_1(v_1^2 + w_1^2) \\ -\vec{v}_1.\nabla\theta_2 - \vec{v}_2.\nabla\theta_1 - u_1.\partial_X\theta_1 \\ 0 \end{bmatrix}$$

References

[1] D.A. Nield, A. Bejan, Convection in Porous Media, Springer-Verlag, New York, 2006.

[2] F. Dufour, M.C. Néel, Numerical study of instability in a horizontal porous channel with bottom heating and forced horizontal flow, Phys. Fluids 10 (9) (1998) 2198–2207.

[3] M. Prats, The effect of horizontal fluid motion on thermally induced convection currents in porous media, J. Geophys. Res. 71 (1967) 4835–4838.

[4] D.A.S. Rees, The effect of inertia on the onset of mixed convection in a porous layer heated from below, Int. Comm. Heat Mass Transfer 24 (2) (1997) 277–283.

[5] A. Delache, M.N. Ouarzazi, M.C. Néel, Structuration de la convection mixte en milieu poreux confiné latéralement et chauffé par le bas : effets d'inertie, C. R. Mécanique 330 (2002) 885–891.

[6] R.J. Briggs, Electron–Stream Interaction with Plasmas, Research Monograph MIT Press, Cambridge, 1964.

[7] A. Bers, Linear waves instabilities, in: C. DeWitt, J. Peyraud (Eds.), Physique des plasmas, Gordon & Breach, 1975, pp. 117–215.

[8] P.A. Huerre, P.A. Monkewitz, Local and global instabilities in spatially developing flows, Annu. Rev. Fluid Mech. 22 (1990) 473–537.

[9] A. Delache, M.N. Ouarzazi, M. Combarnous, Spatio-temporal stability analysis of mixed convection flows in porous media heated from below: comparison with experiments, Int. J. Heat Mass Transfer 50 (2007) 1485–1499.

[10] M. Combarnous, Convection naturelle et convection mixte en milieu poreux, PhD thesis, Faculté des sciences de l'univ. de Paris, 1970.

[11] M. Combarnous, P. Bia, Combined free end forced convection in porous media, Soc. Pet. Eng. J. 251 (11) (1971) 399–405.

[12] M. Combarnous, S.A. Bories, Hydrothermal convection in saturated porous media, in: Advances in Hydroscience, vol. 10, Academic Press, 1975, pp. 231–307.

[13] X. Nicolas, Bibliographical review on the Poiseuille–Rayleigh–Bénard flows: the mixed convection flows in horizontal rectangular ducts heated from below, Int. J. Thermal Sci. 41 (2002) 961–1016.

[14] H.R. Brand, R.J. Dessler, G. Ahlers, Simple model for the Bénard instability with horizontal flow near threshold, Phys. Rev. A 43 (1991) 4262–4268.

[15] H.W. Müller, M. Tveitereid, S. Trainoff, Rayleigh–Bénard problem with imposed weak through-flow: two coupled Ginzburg–Landau equations, Phys. Rev. E 48 (1993) 263–272.

[16] Y. Kato, K. Fujimura, Prediction of pattern selection due to interaction rolls and transverse modes in a flow through a rectangular channel heated from below, Phys. Rev. E 62 (2000) 601–611.

[17] P. Carrière, P.A. Monkewitz, D. Martinand, Envelope equations for the Rayleigh–Bénard–Poiseuille system. Part 1. Spatially homogeneous case, J. Fluid Mech. 502 (2004) 153–174.

[18] A.C. Newell, J.A. Whitehead, Finite bandwidth, finite amplitude convection, J. Fluid Mech. 28 (1969) 279–303.

[19] K. Stewartson, J. Stuart, A nonlinear instability theory for a wave system in plane Poiseuille flow, J. Fluid Mech. 48 (1971) 529–545.

[20] M.N. Ouarzazi, A. Joulin, P.A. Bois, J.K. Platten, Soret effect and mixed convection in porous media, in: W. Köhler, S. Wiegand (Eds.), Thermal Non Equilibrium Phenomena in Fluid Mixtures, in: Lecture Notes in Phys., vol. 584, Springer, 2002, pp. 428–447.

[21] H. Ward, M.N. Ouarzazi, M. Taki, P. Glorieux, Influence of walkoff on pattern formation in nondegenerate optical parametric oscillators, Phys. Rev. E 63 (2000), 016604, 1–13.

[22] A. Delache, Etude analytique et numérique des instabilités spatio-temporelles des écoulements de convection mixte en milieu poreux : comparaison avec l'expérience PhD thesis, Université des Sciences et Technologies de Lille, 2005.

[23] S.S. Chen, A.S. Lavine, Laminar, buoyancy induced flow structures in a bottom heated, aspect ratio 2 duct with throughflow, Int. J. Heat Mass Transfer 39 (1996) 1–11.

[24] U. Narusawa, Mixed convection in a rectangular duct heated from below, Int. J. Fluid Mech. Res. 25 (1998) (1996) 285–294.

[25] M. Combarnous, S. Bories, Modélisation de la convection naturelle au sein d'une couche poreuse horizontale à l'aide d'un coefficient de transfert solide–fluide, Int. J. Heat Mass Transfer 17 (1974) 505–515.

[26] N. Banu, D.A.S. Rees, Onset of Darcy–Bénard convection using a thermal non-equilibrium model, Int. J. Heat Mass Transfer 45 (2002) 2221–2228.

[27] M. Tveitereid, H.W. Müller, Pattern selection at the onset of Rayleigh–Bénard convection in a horizontal shear flow, Phys. Rev. E 50 (1994) 1219–1226.

[28] R.J. Deissler, External noise and the origin and dynamics of structure in convectively unstable systems, J. Statist. Phys. 54 (1989) 1459–1488.

[29] C. Cossu, T. Loiseleux, On the convective and absolute nature of instabilities finite difference numerical simulations of open flows, J. Comput. Phys. 144 (1998) 98–108.